Structural mechanism of the recovery stroke in the Myosin molecular motor

Stefan Fischer*†, Björn Windshügel*‡, Daniel Horak*, Kenneth C. Holmes§, and Jeremy C. Smith¶

Departments of *Computational Biochemistry and ¶Computational Molecular Biophysics, Interdisciplinary Center for Scientific Computing, Universität Heidelberg, 69120 Heidelberg, Germany; and §Max Planck Institut für Medizinische Forschung, 69120 Heidelberg, Germany

Edited by Thomas D. Pollard, Yale University, New Haven, CT, and approved March 7, 2005 (received for review November 24, 2004)

The power stroke pulling myosin along actin filaments during muscle contraction is achieved by a large rotation (≈60°) of the myosin lever arm after ATP hydrolysis. Upon binding the next ATP, myosin dissociates from actin, but its ATPase site is still partially open and catalytically off. Myosin must then close and activate its ATPase site while returning the lever arm for the next power stroke. A mechanism for this coupling between the ATPase site and the distant lever arm is determined here by generating a continuous series of optimized intermediates between the crystallographic end-states of the recovery stroke. This yields a detailed structural model for communication between the catalytic and the force-generating regions that is consistent with experimental observations. The coupling is achieved by an amplifying cascade of conformational changes along the relay helix lying between the ATPase and the domain carrying the lever arm.

chemo-mechanical coupling | conformational transition | Conjugate Peak Refinement | muscle contraction | power stroke

The myosin II head is a molecular motor that transforms chemical energy derived from the hydrolysis of ATP into mechanical work. The myosin head (or cross bridge) contains the catalytic activity, but the release of hydrolysis products is inhibited unless actin is bound. Lymn and Taylor (1) first proposed the cyclic scheme for the interaction between myosin and actin that produces motion (Fig. 1*A*). Underlying this cycle is myosin's ability to couple small changes in its catalytic ATPase site to large conformational changes in both the actin-binding and the distant force-generating domains with well defined communication mechanisms, which ensure that these changes are correlated so as to efficiently produce mechanical work. For instance, the communication mechanism between the ATP and actin-binding regions has been illuminated recently by crystal structures of the unconventional myosin V (2, 3). Here, we focus on one of the other essential communication pathways, the one for passing structural information between the ATPase site and the distant force-generating domain during the recovery stroke of the contractile cycle (i.e., going from states II to III in Fig. 1*A*).

The presence of that coupling first becomes apparent when comparing the crystallographic structures of the two end-states of the recovery-stroke (Fig. 1 *B* and *C*) (4, 5). As expected, the largest difference between these structures is in the orientation of the "converter" domain, which carries the lever arm and which is rotated by ≈60° relative to the rest of the head (referred to hereafter as the "main body"). The other significant difference is in the ATP binding site, which is partially open before the recovery stroke, rendering the ATPase catalytically inactive (for example, see figure 6a in ref. 6). In contrast, after the recovery stroke, the ATP site is fully closed and the γ-phosphate (γP) group of the ATP forms an additional hydrogen bond with the amide of Gly-457 (*Dictyostelium discoideum* numbering). Gly-457 is located on a conserved loop called the Switch-2 element, which is displaced ≈5 Å toward γP in the postrecovery-stroke conformation, allowing the formation of a salt bridge between residues Glu-459 and Arg-238. This salt bridge and the hydrogen bond of γP to Gly-457 are instrumental in closing the active site and switching on the catalytic ATPase function (6).

The recovery stroke is not driven by the ATP binding energy. Indeed, kinetic studies have shown that myosin can freely exchange between the end states of the recovery stroke in the presence of ATP (7), and structures with a bound ATP analogue (ADP.BeF3) have been crystallized also in the prerecovery-stroke conformation (4). However, it would be wasteful if the ATPase site could freely close and reopen with the lever arm still in the prerecovery orientation, allowing ATP hydrolysis and unproductive product release. Therefore, a mechanism is likely to couple the closing of the ATPase site with the reorientation of the lever arm. Because these two structural elements are more than 40 Å apart (see Fig. 1*B*), the communication mechanism between them cannot be inferred directly from the crystallographic end states of the recovery stroke.

To generate a series of intermediate structures of the recovery stroke that are meaningful at the atomic level of detail, a low-energy path of the conformational transition has been computed here by using the Conjugate Peak Refinement (CPR) method (8). CPR allows every atom in the protein to move independently and does not use external constraints to drive the transition. CPR has been shown to allow the determination of complex processes in proteins (9–13). The result of the CPR calculation is a continuous series of myosin structures that connects the crystallographic end states of the recovery stroke (see *Methods*). This is similar to a molecular dynamics trajectory, except that when viewed in sequence, it yields molecular "movies" that show only the motions that are essential for the transition (see Movies 1–4, which are published as supporting information on the PNAS web site). These transition intermediates reveal a mechanism for the mechanical coupling of the recovery stroke and show how a small motion in the ATPase site is gradually amplified into a large-scale domain motion. A sequence of structural changes cascading along the relay helix which runs from the ATP-binding site to the converter domain (see Fig. 1 *B* and *C*) results in the essentially rigid-body rotation of the converter domain and the lever arm. The order of these events is sterically logical and is consistent with available experimental observations, such as the phenotype of several point mutations.

Methods

Transition End States. The myosin head from *D. discoideum* in the absence of actin has been crystallized with various ligands bound in the active site. For the prerecovery-stroke conformation (Fig. 1*B*), Protein Data Bank (PDB) entry 1MMD was used (4). For the postrecovery-stroke conformation (Fig. 1*C*), a crystal struc-

This paper was submitted directly (Track II) to the PNAS office.

Abbreviations: γP, γ phosphate; CPR, Conjugate Peak Refinement; SH1, Src homology 1.

†To whom correspondence should be addressed. E-mail: stefan.fischer@iwr.uni-heidelberg.de.

‡Present address: Institut für Pharmazeutische Chemie, Martin-Luther-Universität Halle-Wittenberg, 06120 Halle (Saale), Germany.

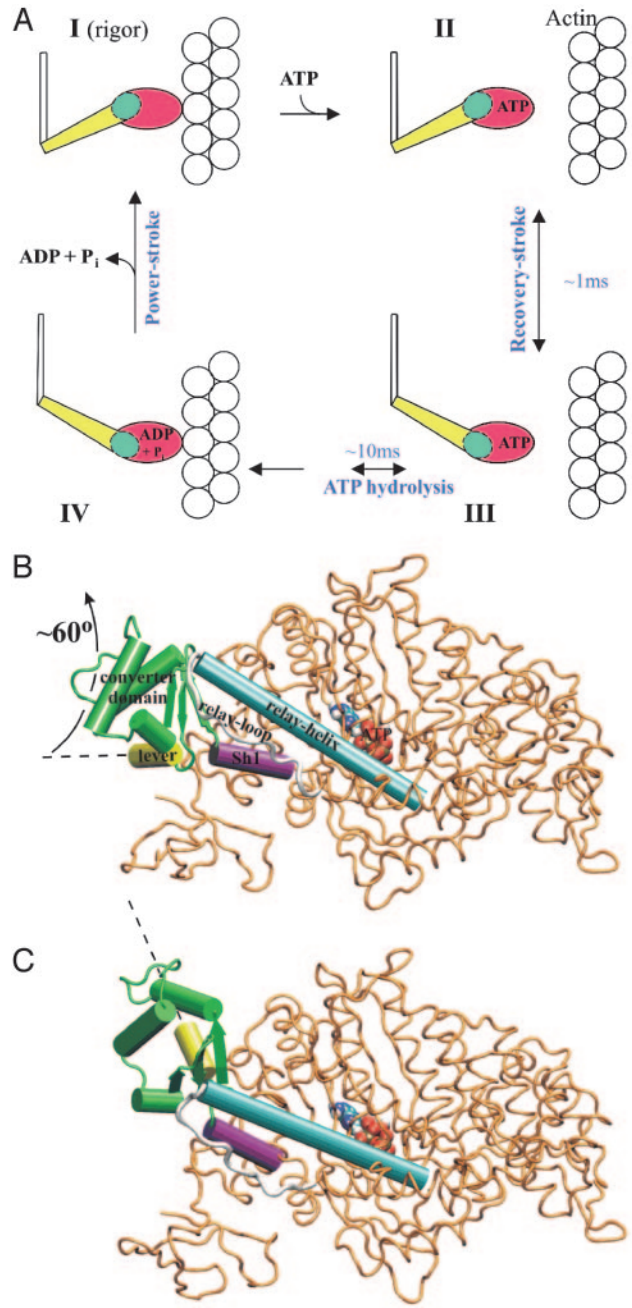

Fig. 1. The recovery stroke. (*A*) The Lymn–Taylor contraction cycle (1, 6). (I) After a power stroke, the lever arm (in yellow) of myosin is ''down'' with respect to the main body of the myosin head (in red), which binds strongly to the actin filament (white spheres). The lever arm forms a rigid unit with the converter domain (green) and is attached flexibly to the myosin filament (white rectangle). (II) ATP binding to the main body provokes its dissociation from actin. The ATP site is partially open (4) and catalytically inactive (6). (III) The recovery stroke brings the lever arm ''up'' into the prepower stroke orientation, while closing the ATP binding site, thereby making the ATPase catalytically active. (IV) ATP hydrolysis remains reversible until myosin binds strongly to actin (29). The lever arm then rows the myosin fibril along the actin filament while irreversibly releasing phosphate and ADP. (*B*) Prerecovery-stroke conformation of the myosin head (state II of the cycle) (3). The converter domain (green) carries the lever arm helix (yellow, shown truncated). (*C*) Postrecovery-stroke conformation (state III) (4). The converter domain orientation relative to the main body (orange, oriented as in *A*) differs by 60–65° relative to the prerecovery conformation. In state IV (not shown), actin binds from the right. ATP is shown in van der Waals representation. Important elements for the coupling mechanism are the relay helix (cyan, residues 466–498), the relay-loop (white, 499–509), and the SH1-helix (purple, 681–690).

ture very similar to PDB entry 1VOM was used (5), but the structure provides coordinates for the converter domain (Jon Kull, personal communication). In both end states, ATP was modeled by replacing the BeF_3 of the bound Mg-ADP-BeF_3 with a phosphate group. Modeling of a missing segment in 1MMD (residues 501–507) was based on the 2MYS structure (14), using MOLOC and its MAB force field for geometry optimization (15). Because 1MMD misses the nonessential residues 16–35, these were deleted also in the postrecovery-stroke conformation. A total of 31 buried water molecules present in both crystal structures were included. Calculations were performed by using the molecular mechanics program CHARMM (16) with force-field parameter sets 19 for nonaromatic groups and 22 for the aromatic groups (17). A distance-dependent dielectric constant was used to approximate solvent screening. Overall, end states changed little upon minimization. In the prerecovery-stroke conformation, the relay helix is bent more and the converter domain rotated more (65° relative to postrecovery) than in the crystal (in which it is only 60°), suggesting that crystal contacts may have prevented maximal converter rotation in 1MMD. Interestingly, the salt bridge between Glu-459 and Arg-238, which is broken in prerecovery-stroke crystal structures, formed spontaneously upon minimization in presence of ATP, reducing the Gly-457/γP distance from 7 to 5.1 Å and thus initiating the recovery stroke transition.

Molecular Kinematics. The time scale of the recovery stroke is in the 1- to 10-ms range (7), beyond the scope of standard, unconstrained molecular dynamics simulations. Applying constraints along some predefined reaction coordinate to accelerate the simulation (18) tends to favor events correlating strongly with this predefined reaction coordinate, thus biasing the sequence of events upon which a description of the mechanism is to be based. Therefore, the recovery stroke was simulated here by molecular kinematics, which gives a time-independent but energetically correct description of the process in the form of a minimum energy path (MEP) connecting the two end conformations. A MEP consists of a series of energy-optimized structures of the protein, which constitute a continuous trajectory in conformational space that follows the streambed of the multidimensional energy surface. Unlike a description given by ''morphing'' (19), the MEP goes through optimized transition-state structures (which are first-order saddle points of the energy surface), thus ensuring that the path is kinetically accessible. Here, the MEP was calculated by using the CPR method (8) as implemented in the TREK module of CHARMM, starting from an initial guess of the path, which was built by combined interpolation in Cartesian and internal coordinates with side chain shrinking (as described in ref. 13), and leaving all 7,986 atoms free to move independently. The resulting pathway of the recovery stroke consists of ≈1,200 protein structures (shown in Movies 1–4).

Results

Domain Motion. First we describe the large (≈65°) rotation of the converter domain relative to the main body of the myosin head (Fig. 2 *Left*). Because the N-terminal segment of the lever-arm helix is an integral part of the converter domain, the lever-arm rotates by the same amount. Although full internal flexibility was allowed in the calculations, the converter domain does not change its internal structure during the transition, acting as a semirigid body. The converter domain is attached to the main body by the polypeptide chain at the Src homology 1 (SH1) helix. This connection point serves as a hinge for the converter rotation, involving a partial corotation of the SH1 helix and changes in the backbone dihedral angles at the SH1/converter junction (for example, ϕ_{Arg689}, ψ_{Lys690}, and ϕ_{Gly691} increase by 26°, 34°, and 31°, respectively). The importance of changes in this

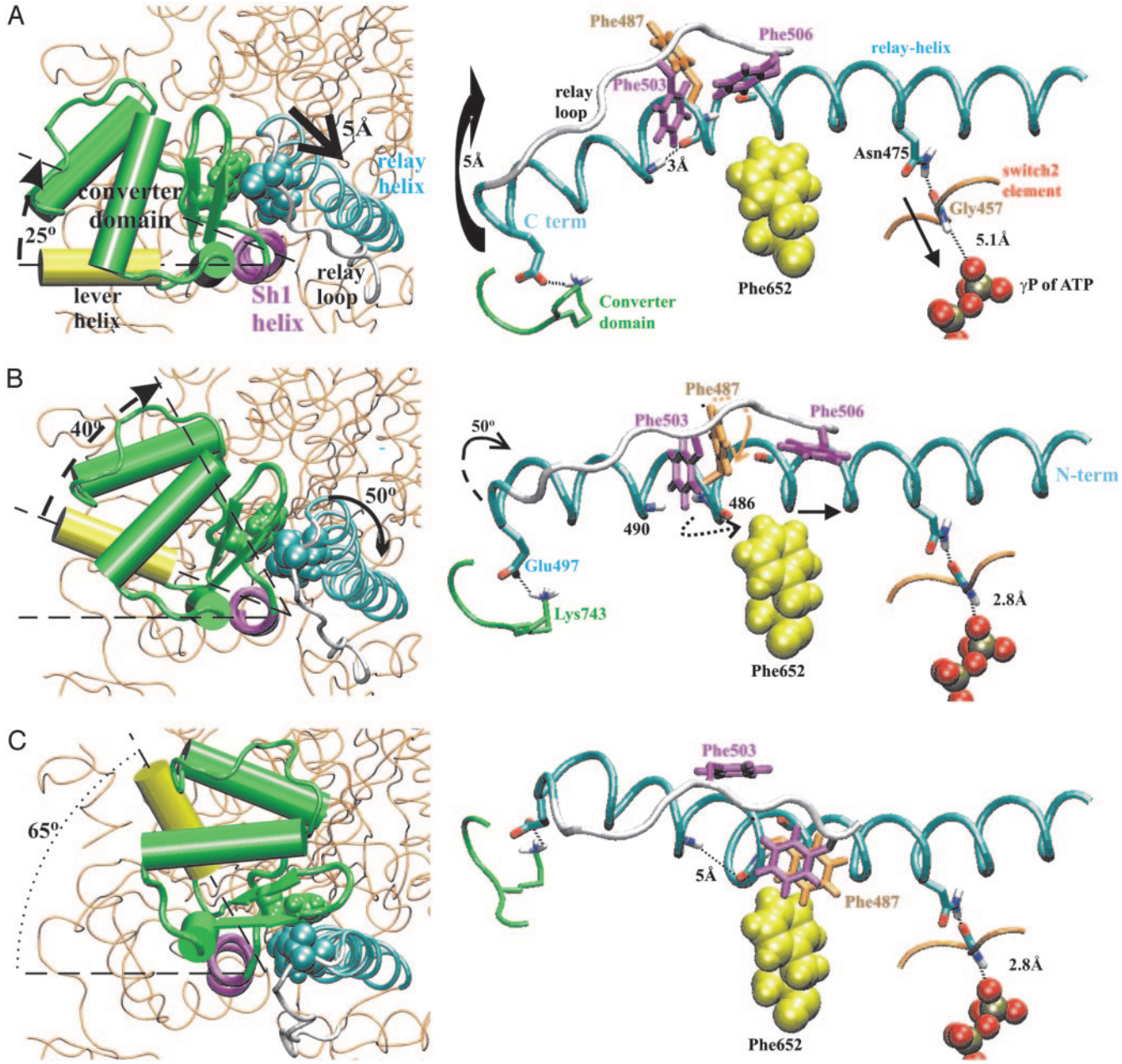

Fig. 2. Coupling mechanism. (*Left*) The converter domain rotation, viewed from the C terminus of the relay helix and down the axis of the SH1 helix, whose axis is similar to the converter-rotation axis. The main body (in orange, same orientation in the three panels) moves little. (*Right*) The changes along the relay helix that couple the small motion of the Switch-2 with the large translation of the helix C terminus. See Movies 3 and 4. (*A*) Prerecovery stroke state (same conformation and colors as Fig. 1*B*). The lever-arm helix (in yellow in *Left*) is down. Motion of Gly-457 toward the γ-phosphate (thin arrow in *Right*) pulls the relay helix via the Asn-475 side chain, unbending and lifting the helix C terminus 5 Å (thick arrows) by a seesaw-like pivoting of the helix over its fulcrum at Phe-652 (in yellow), thereby causing the converter domain (and the lever helix) to pivot by ≈25°. (*B*) Conformation halfway along the transition. Throughout, the C terminus of the relay helix maintains its interactions with the converter domain (Tyr-494 and Ile-499 in cyan packing against Phe-745 in green, *Left*; Lys-743-Glu-497 salt bridge, *Right*), thus controlling the rotation of the converter domain. The pull toward ATP cannot pivot the relay helix further, inducing strain near the fulcrum (straight arrow in *Right*). This breaks the ≈486–490 intrahelical hydrogen bond (dotted arrow), favoring the reorientation of Phe-487 (orange arrow), which partially unwinds the relay helix near 486 and rotates the C-terminal half of the helix by ≈50° around its own axis (curved arrow shown in *Left* and *Right*). This rotation causes the converter domain to pivot by a further 40° (*Left*). (*C*) Postrecovery-stroke conformation (same as Fig. 1*C*). The converter domain has fully rotated and the lever-arm helix is 65° up (*Left*). Phe-487 has completed its reorientation and packs against Phe-506 (*Right*).

region had been mentioned (6), and the G691A mutation was shown to cause some uncoupling of the ATPase (20). The axes of the SH1 and lever-arm helices intersect in the two end states (see Fig. 2 *A* and *C Left*), and do so also throughout the pathway (Fig. 2*B Left*), such that the rotation axis can be viewed approximately parallel to the SH1 helix axis (see Movie 3).

In both crystallographic end states, the converter makes contact with the C terminus of the relay helix via salt bridges and hydrophobic interactions (Fig. 2 *A* and *C*). The transition shows that these contacts are maintained during the whole recovery stroke (Fig. 2*B*), as the C terminus of the relay helix translates by up to 11 Å, closely accompanying the converter-domain rotation (Fig. 3*A*). This translation is achieved by conformational changes in the relay helix, which first unbends

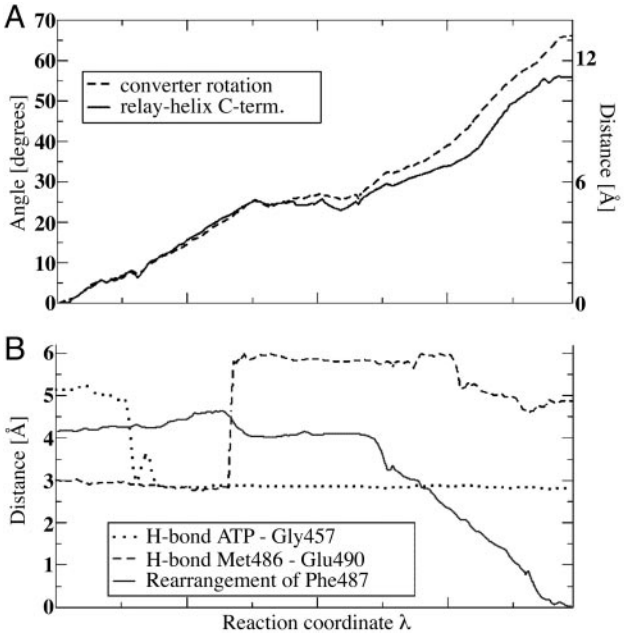

Fig. 3. Sequence of events along the transition. (*A*) Synchronous progress of converter-domain rotation (angle on left axis, dashed line) and translation of the relay helix C terminus (distance on right axis, solid line). (*B*) Successive events: (*i*) Formation of the hydrogen bond between Gly-457 and the γ-phosphate of ATP (N_{457}-O_γ distance, dotted line), see Fig. 2*A Right*. (*ii*) Breaking of the relay helix intrahelix hydrogen bond between Met-486 and Glu-490 (dashed line), see Fig. 2*B*. (*iii*) Translation of Phe-487 (solid line), see Fig. 2*C*. The reaction coordinate λ measures the overall progress of the transition (r.m.s. difference in all atomic coordinates between successive intermediates, summed along the transition).

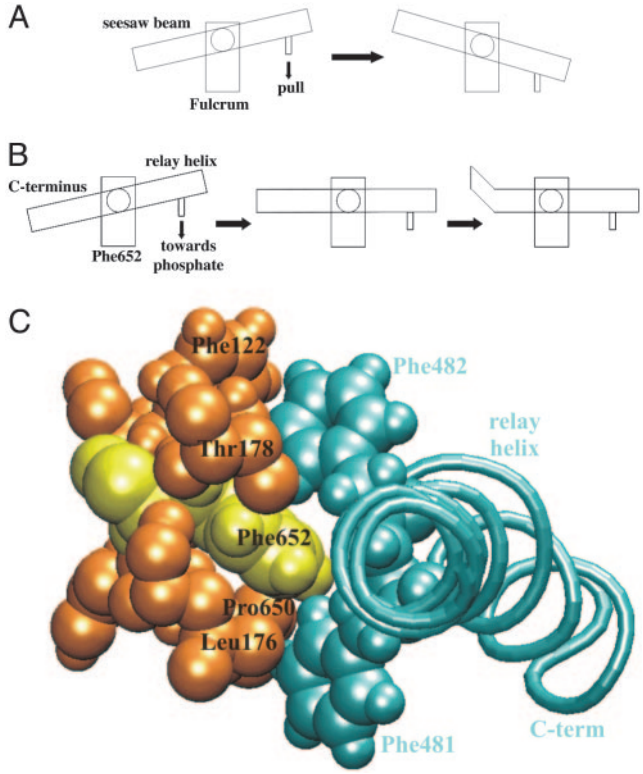

Fig. 4. The seesaw mechanism. (*A*) Pulling on the beam of a seesaw causes it to pivot over its fulcrum. (*B*) Pulling on the relay helix causes it to pivot about its fulcrum at Phe-652, leading first to unbending of the helix, then to helix strain and untwisting (at Phe-487). In sum, these provoke a large upswing of the helix C terminus. The power stroke is thought to reverse this sequence of events. (*C*) The molecular fulcrum, viewed here along the axis of the N-terminal half of the relay helix (cyan), consists of the tight interlocking between two residues (Phe-481 and Phe-482) on this helix and Phe-652 (yellow) located on a central β-sheet of the main body (orange). Several hydrophobic residues surround Phe-652 and further stabilize the fulcrum. This hydrophobic core remains locked during the whole transition.

(Fig. 2 $A \rightarrow B$) and then partially unwinds (Fig. 2 $B \rightarrow C$). Because the contacts between the relay helix and the converter domain are maintained, the rotation of the converter domain is determined by the changes in the relay helix and vice versa. Thus, understanding the ATPase/lever-arm coupling is equivalent to understanding why the relay helix responds as it does to changes in the ATP-binding site.

The Seesaw Phase. Here and below, we describe the cascade of structural events along the relay helix that couple the ATPase site and the converter domain. Two phases can be distinguished along the transition, which we call the "seesaw" and the "unwinding" phases, each referring to a conformational change of the relay helix. The seesaw phase is initiated by the spontaneous formation of the salt bridge between Glu-459 and Arg-238 (see *Methods*). This bridge pulls Gly-457 closer to γP by ≈2.5 Å (data not shown) and is immediately followed by a 2.3-Å movement of the Gly-457/Ser-456 peptide group toward the γP (Fig. 3*B*), with which it forms a hydrogen bond (Fig. 2 *A Right*). This hydrogen bond is believed to be essential for the myosin ATPase function, because it positions the γP in the active site and facilitates the attack by a nucleophilic group that leads to the cleavage of the βP-γP bond. Once formed, this hydrogen bond is stable throughout the remaining transition (see Fig. 3*B*).

The Gly-457/Ser-456 peptide group also is engaged in a hydrogen bond with the side chain of Asn-475, located on the N-terminal half of the relay helix (Fig. 2 *Right*). This hydrogen bond, which is present in both end states, is maintained at all times during the transition. Thus, when the Gly-457/Ser-456 peptide group moves toward the γP, it pulls on Asn-475, which is therefore displaced in the same direction. Consequently, the net effect of the hydrogen bond formed between Gly-457 and γP is to pull on the relay helix at position 475, via the hydrogen-bonded bridge γP···Gly-457/Ser-456···Asn-475/relay-helix (Fig. 2*A Right*). This pull on Asn-475 triggers a series of structural changes along the relay helix. The first response of the relay helix is a motion resembling that of a seesaw (Fig. 4 *A* and *B*): pulling down one end of the seesaw beam (the relay helix N-terminal segment) leads to upswing of the opposite end (the C-terminal segment). The seesaw fulcrum is formed by three interlocked phenylalanine side chains (Fig. 4*C*): Phe-652 of the main body, straddled by Phe-481 and Phe-482 of the relay helix. Together, they constitute a well defined pivoting point for the relay helix. The C terminus of the relay helix swings up by 5 Å (Fig. 2*A*), so that the helix goes from a bend to a straight conformation (Fig. 4 $A \rightarrow B$). During this upswing, the converter domain rotates by 25° (Fig. 3*A*), pulled along by its contacts with the relay helix C terminus.

The Unwinding Phase. In the second phase of the transition, further seesaw motion is hindered by the fact that the relay helix is not a freely pivoting beam, but is anchored at its N terminus by the continuing polypeptide backbone. Thus, the continued pull on Asn-475 toward γP results in strain near the fulcrum, stretching intra-helix hydrogen bonds until the helical hydrogen bonds 486···490 and 483···487 break due to a flip of the 486/487 peptide group (see Fig. 2*B Right*). The 486···490 hydrogen bond remains broken for the rest of the transition (Fig. 3*B*). These

defects in the helix H-bonding allow a local unwinding of the relay helix, involving a register shift of the helix hydrogen bond pattern from $n + 4$ (normal α–helix) to $n + 5$ for three pairs of residues (483···488, 484···489 and 485···490, not shown). During this unwinding of the relay helix, the C-terminal helix half rotates lengthwise by about 50° (see Fig. 2 $B \rightarrow C$), rolling on the SH1 helix and introducing a kink half-way along the relay helix (at the level of residue 486). This translates the C terminus of the relay helix by a further 6Å (Fig. 3*C*). The helix terminus remains in contact with the converter domain, thus resulting in a further 40° rotation of the converter domain (Fig. 2 $B \rightarrow C$ *Left*). This completes the overall converter-domain rotation and brings the lever-arm into its final prepower-stroke orientation.

The unwinding of the relay helix depends on the change in packing of two aromatic residues located half way along the relay helix, Phe-487 and Phe-506, which adopt very different conformations in the crystallographic end states (compare the right panels of Fig. 2 *A* and *C*). The side chain that is instrumental in coupling this "aromatic switch" with relay helix unwinding is Phe-487, which is carried by the relay helix and reorientates from a solvent-exposed to a buried position. During the transition, the side chain of Phe-506 first rotates aside and Phe-487 transiently packs against Phe-503 (Fig. 2*B Right*). Then, Phe-487 passes between the relay helix and the relay loop (see Movie 4) and finally packs against Phe-506 (and Phe-482, not shown). This passage is not possible in the prerecovery-stroke conformation, in which the relay loop is packed against the relay helix and blocks the passage of Phe-487. The present transition intermediates show the passage of Phe-487 to occur progressively during the helical unwinding phase (Fig. 3*B*), but only after structural changes during the preceding seesaw phase have opened the passage in two ways: (*i*) The 5-Å translation of the relay helix C terminus has increased the space between the helix and the relay loop (compare Fig. 2*A Left* with *B Left*) and (*ii*) the reorientation of Phe-506 has enabled Phe-487 to pass between Phe-503 and Phe-506 (Fig. 2*B Right*). These two events in the seesaw phase must precede the aromatic switch and the unwinding of the relay helix. Thus, the order of events presented here is necessary from a steric point of view.

Discussion

The coupling between converter domain orientation and the closing of Switch-2 over the ATP makes it less likely that ATP is hydrolyzed without a productive contraction cycle. The present results show how small structural changes in the ATP binding site can be amplified into a large domain rotation, and vice versa, via the relay helix. Two phases can be distinguished. The first, seesaw phase is initiated by the pulling of Gly-457 toward the γP of ATP, favoring partial unbending of the relay helix by the seesaw effect and rotation of the converter domain by ≈25°. A molecular fulcrum anchors the relay helix on the main body of the myosin head (at Phe-652) and provides a pivoting point for the seesaw motion. Straightening of the relay helix provokes strain at the fulcrum, leading to the breaking of helix hydrogen bonds near the fulcrum. The second, unwinding phase is governed by the local helical unwinding of the relay helix near the seesaw fulcrum and depends on the reorientation of Phe-487, which acts like a lever and packs against Phe-506 after the recovery stroke. In some myosins (for example, mammalian Ia and Ib), Phe-487 is replaced by Leu, whose large hydrophobic side chain could play a similar lever role, and Phe-506 is replaced by Tyr, which allows for a similar packing. Together, the seesaw effect and helical unwinding result in a large translation (≈11 Å) of the C-terminal helix end, which is connected throughout the transition to the converter domain by noncovalent interactions. This translation thus leads to the ≈60° rotation of the converter domain around an axis described approximately by the SH1–helix axis.

The proposed coupling mechanism is consistent with all of the following experimental observations. First, it explains the finding that the mutation of Ser-456 to leucine reduces the step size of myosin walking along the actin filament (21). The present mechanism suggests that the larger leucine side chain in this mutant should hinder the movement of the 456/457 peptide group toward γP in the S456L mutation during the seesaw phase (Fig. 2*A*), leading to a reduced pull on Asn-475 and to a reduced upswing of the relay helix, and therefore to a smaller rotation of the converter domain. Another observation, that the mutation of either Phe-487 to alanine or Phe-506 to glycine uncouples the ATPase activity from the lever-arm motion (22), strongly supports the present proposal that the Phe-cluster located halfway along the relay helix (Fig. 2) plays an essential role in transmitting the structural information from the ATP binding site to the converter domain. A further observation is that the relay loop (shown in white in Fig. 2), which continues the polypeptide chain after the relay helix, is often disordered in crystal structures. This flexibility makes sense in the context of the coupling mechanism proposed here. First, the motion of the relay helix C-terminal half should not be impeded by a tightly ordered relay loop. Second, Phe-487 must in any case pass between the relay helix and the relay loop (see Fig. 2). This passage would be difficult if the relay loop were well structured and packed against the relay helix. Finally, cross-linking experiments have shown that the relay helix and the converter domain remain in contact throughout the whole contraction cycle (23). This finding is also consistent with the present mechanism, which exhibits a conserved interdomain linkage throughout the transition. Both electrostatic and hydrophobic interactions may contribute to this noncovalent link. Sequence comparisons between different myosins point to the importance of the hydrophobic interactions (6). Indeed, the hydrophobic cluster at the relay helix/converter junction (Fig. 2 *Left*) is maintained in all transition intermediates. However, a salt bridge is also present throughout the transition (Fig. 2 *Left*), and the breaking of interdomain salt bridges can involve large free-energy barriers (24), thus contributing to stabilize domain junctions.

The coupling model proposed here can be tested experimentally because it predicts the phenotype of several point mutations. For instance, one element of the mechanism is the transmission through the Asn-475 side chain of the pull by the γP on Gly-457 into a pull on the relay helix (Fig. 2*A Right*). If Asn-475 were mutated to a nonpolar residue, the hydrogen bond between Asn-475 and the 456/457 peptide group would be absent. Consequently, this would lessen the pull on the relay helix and might uncouple ATP hydrolysis from lever-arm motion. At the same time, it might also reduce the ATPase activity in the closed state, due to a poorer positioning of the catalytically important Gly-457 amide in absence of the hydrogen bond to the Asn-475 side chain. Another important element of the mechanism is the fulcrum, which could be examined by mutation of the three Phe residues forming its core (Fig. 4*C*). For example, mutation of Phe-652 to a small residue (e.g., glycine) should destroy the function of the fulcrum, because there would be no anchoring point for the relay helix. The same might be achieved by double mutation of Phe-481 and Phe-482 to glycines. The expected phenotypes would be either decoupling of ATPase activity and lever-arm motion or a reduced step size.

Trp-501 is the natural fluorescent probe that has been used to monitor relay helix movement (20); thus, it is interesting to examine its behavior during the recovery stroke. In addition to a halving of the solvent accessible surface of the Trp-501 indole, comparison of the end states shows that the major change is the formation of a perfect H-bond between the indole and the side chain of Gln-491, which has to approach by ≈10 Å. This H-bond can only form after Phe-487 has passed between relay helix and relay loop, i.e., after the relay helix has started unwinding. This

behavior would be consistent with Trp-501 being such a good signal for the recovery stroke transition, if Gln-491 was responsible for the fluorescence change; this can be tested by mutating Gln-491 into a nonpolar residue.

The flow of structural change has been described above in the direction ATP → lever arm. However, the coupling mechanism is also valid in the reverse direction, i.e., a motion in the converter domain can lead to the corresponding modifications near ATP. The coupling simply ensures that whenever the lever arm is in prepower-stroke position, the ATPase function is switched on, and when it is in the prerecovery-stroke position, the ATPase function is switched off. It is plausible that some elements of the coupling mechanism described here might be active during the power stroke, although this is not to imply micro reversibility, because the power stroke occurs in a different, actin bound, conformation. In particular, the aromatic switch and the packing of Phe-487 may play a similar role in "rewinding" (unkinking) the relay helix, in a reversal of the unwinding process that has been described here. Also, for the same steric reasons given above (i.e., the space needed for Phe-487 to pass between the relay helix and the relay loop), the relative order of main events is likely to be reversed, such that the rewinding of the relay helix precedes its "bending" (reversed seesaw motion) during the power stroke. However, other mechanisms must also be at work during the power stroke to produce force. The recent myosin V structures (2, 3) and a high-resolution cryoelectron microscopic structure of the rigor actomyosin complex (25) suggest that strong binding to actin is correlated with a twisting of the central β-sheet of myosin, which might relieve the pressure on the relay helix, thus inducing the relay helix to rewind (unkink) and provoking the power stroke motion of the converter domain (26, 27). This would mean that actin binding controls the power stroke. Computation of the transition intermediates between these structures will help to better understand the mechanism of communication between the actin binding domain and the relay helix.

We thank Jon Kull for the crystal structure and helpful discussions. The figures were made with the program VMD (28). This work was supported by Deutsche Forschungsgemeinschaft Grant SM63/3.

1. Lymn, R. W. & Taylor, E. W. (1971) *Biochemistry* **25,** 4617–4624.
2. Coureux, P. D., Wells, A. L., Menetrey, J., Yengo, C. M., Morris, C. A., Sweeney, H. L. & Houdusse, A. (2003) *Nature* **425,** 419–423.
3. Coureux, P. D., Sweeney, H. L. & Houdusse, A. (2004) *EMBO J.* **23,** 4527–4537.
4. Fisher, A. J., Smith, C. A., Thoden, J. B., Smith, R., Sutoh, K., Holden, H. M. & Rayment, I. (1995) *Biochemistry* **34,** 8960–8972.
5. Smith, C. A. & Rayment, I. (1996) *Biochemistry* **35,** 5404–5417.
6. Geeves, M. A. & Holmes, K. C. (1999) *Annu. Rev. Biochem.* **68,** 687–728.
7. Malnasi-Csizmadia, A., Pearson, D., Kovacs, M., Woolley, R. J., Geeves, M. A. & Bagshaw, C. R. (2001) *Biochemistry* **40,** 12727–12737.
8. Fischer, S. & Karplus, M. (1992) *Chem. Phys. Lett.* **194,** 252–261.
9. Dutzler, R., Schirmer, T., Karplus, M. & Fischer, S. (2002) *Structure (London)* **10,** 1273–1284.
10. Bondar, A. N., Elstner, M., Suhai, S., Smith, J. C. & Fischer, S. (2004) *Structure (London)* **12,** 1281–1288.
11. Fischer, S., Michnick, S. & Karplus, M. (1993) *Biochemistry* **32,** 13830–13837.
12. Sopkova, J., Fischer, S., Guilbert, C., Lewit-Bentley, A. & Smith, J. C. (2000) *Biochemistry* **39,** 14065–14074.
13. Noe, F., Ille, F., Smith, J. C. & Fischer, S. (2005) *Proteins* **59,** 534–544.
14. Rayment, L., Rypniewski, W. R., Schmidt-Base, K., Smith, R., Tomchick, D. R., Benning, M. M., Winkelmann, D. A., Wesenberg, G. & Holden, H. M. (1993) *Science* **261,** 50–58.
15. Gerber, P. R. & Müller, K. (1994) *J. Comp. Aid. Mol. Design* **9,** 251–268.
16. Brooks, B. R., Bruccoleri, R. E., Olafson, B. D., States, D. J., Swaminathan, S. & Karplus, M. (1983) *J. Comp. Chem.* **4,** 187–217.
17. Neria, E., Fischer, S. & Karplus, M. (1996) *J. Chem. Phys.* **105,** 1902–1921.
18. Schlitter, J., Engels, M. & Kruger, P. (1994) *J. Mol. Graphics* **12,** 84–89.
19. Krebs, W. G. & Gerstein, M. (2000) *Nucleic Acids Res.* **28,** 1665–1675.
20. Batra, R. & Manstein, D. J. (1999) *Biol. Chem.* **380,** 1017–1023.
21. Murphy, C. T., Rock, R. S. & Spudich, J. A. (2001) *Nat. Cell. Biol.* **33,** 311–315.
22. Tsiavaliaris, G., Fujita-Becker, S., Batra, R., Levitsky, D. I., Kull, J. F., Geeves, M. A. & Manstein, D. J. (2002) *EMBO Rep.* **3,** 1099–1105.
23. Shih, W. M. & Spudich, J. A. (2001) *J. Biol. Chem.* **276,** 19491–19494.
24. Gruia, A. D., Fischer, S. & Smith, J. C. (2002) *Proteins* **50,** 507–515.
25. Holmes, K. C., Angert, I., Kull, F. J., Jahn, W. & Schroder, R. R. (2003) *Nature* **425,** 423–427.
26. Holmes, K. C., Schröder, R. R., Sweeney, H. L. & Houdusse, A. (2004) *Philos. Trans. R. Soc. London B* **359,** 1819–1828.
27. Sweeney, H. L. & Houdusse, A. (2004) *Philos. Trans. R. Soc. London B* **359,** 1829–1841.
28. Humphrey, W., Dalke, A. & Schulten, K. (1996) *J. Mol. Graphics* **14,** 33–38.
29. Dale, M. P. & Hackney, D. D. (1987) *Biochemistry* **26,** 8365–8372.